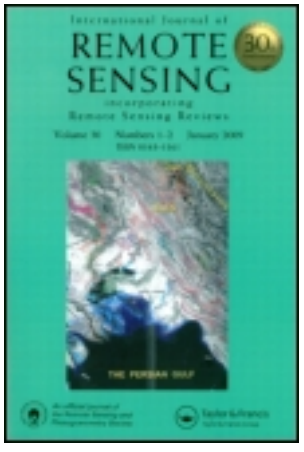

International Journal of Remote Sensing
Publication details, including instructions for authors and subscription information:
http://www.tandfonline.com/loi/tres20

Line-based rational function model for high-resolution satellite imagery

Tee-Ann Teo [a]

[a] Department of Civil Engineering , National Chiao Tung University , Hsinchu , 30010 , Taiwan

Published online: 08 Oct 2012.

To cite this article: Tee-Ann Teo (2013) Line-based rational function model for high-resolution satellite imagery, International Journal of Remote Sensing, 34:4, 1355-1372, DOI: 10.1080/01431161.2012.720044

To link to this article: http://dx.doi.org/10.1080/01431161.2012.720044

International Journal of Remote Sensing
Vol. 34, No. 4, 20 February 2013, 1355–1372

Taylor & Francis
Taylor & Francis Group

Line-based rational function model for high-resolution satellite imagery

Tee-Ann Teo*

Department of Civil Engineering, National Chiao Tung University, Hsinchu 30010, Taiwan

(*Received 14 February 2011; accepted 14 November 2011*)

The object-to-image transformation of high-resolution satellite images often involves a rational functional model (RFM). Traditionally, RFM uses point features to obtain the transformation coefficients. Since control lines offer greater flexibility than control points, this study proposes a new RFM approach based on linear features. The proposed methods include direct RFM and bias-compensated RFM using control lines. The former obtains the rational polynomial coefficients (RPCs) directly from control lines, whereas the latter uses sensor-orientated RPCs and control lines to determine compensated coefficients. The line-based RFMs include vector and parametric line representations. The experiments in this study analysed the effects of line number, orientation, and length using simulation and real data. The real data combined three-dimensional building models and high-resolution satellite images, such as IKONOS and QuickBird images. Experimental results show that the proposed algorithms can achieve pixel-level accuracy.

1. Introduction

1.1. Motivation and goals

Many commercial satellites can provide images with sub-metre spatial resolution. Recent improvements in spatial resolution have increased the applications of satellite images. Some of these methods integrate different types of data to reveal more information. Two examples of these applications are the fusion of spectral and surface data for land-cover classification and the combination of spectral and vector data for change detection. The first step of data fusion transforms all data into a unified coordinate system. Each point in this coordinate system contains different types of information. Hence, the accuracy of data co-registration plays an important role in the data fusion process.

Data co-registration generally includes two major steps: selecting control features and transformation models (Zitova and Flusser 2003). Control features are used to solve the coefficients of transformation models. Control entities include control points (Grussenmeyer and Khalil 2002), control lines (Akav, Zalmanson, and Doytsher 2004; Jung and Boldo 2004; Habib et al. 2005), and control surfaces (Jaw 2000). Control points represent a set of two-dimensional (2D) point features in the image space and three-dimensional (3D) point features in the object space. Point features have been recognized as more robust control entities than other entities. Researchers have designed many transformation models, such as co-linearity equations, to control point features. However, point features have

*Email: tateo@mail.nctu.edu.tw

ISSN 0143-1161 print/ISSN 1366-5901 online

http://dx.doi.org/10.1080/01431161.2012.720044
http://www.tandfonline.com

fewer geometric attributes than other entities. Control lines include sets of 2D line features in the image space and 3D line features in the object space. These linear features primarily appear in buildings, roads, and other man-made objects. These features are usually used in conjunction with 2D image and 3D vector data when point features are difficult to measure, such as occlusions created by building corners. Control surfaces represent a set of co-planar features in the image space and corresponding 3D surface models and are usually used in conjunction with 2D image and 3D lidar point clouds.

Photogrammetric studies often use control points as basic control features. In some scenarios, linear features are easier to measure than point features. Hence, photogrammetric studies often use linear features in addition to point features. Advanced digital image processing techniques can extract linear features from the image space using edge detectors and line extraction methods. Linear features in the object space can also be obtained from existing vector data. Therefore, the advantage of using linear features is that they improve the efficiency of measuring control features. The two measured points on the line segments in image and object spaces do not have to be conjugate points. In other words, the length of the control line in the image and object spaces can be different. Control lines have been successfully used in many photogrammetric applications, including orientation modelling (Karjalainen, Hyyppa, and Kuittinen 2006), camera calibration (Habib, Morgan, and Lee 2002), and image registration (Al-Ruzouq 2010).

Transformation models between 2D image space and 3D object space for satellite imagery can be classified into two categories: physical models and mathematical models. Physical models (Poli, Zhang, and Gruen 2004) use co-linearity equations to describe the relationship between the 2D image and 3D object spaces. Although physical models provide meaningful parameters, their dynamic sampling involves many mathematics calculations that require a lot of computation time. The rational function model (Tao and Hu 2002) is a mathematical model that was successfully applied to several high-resolution satellite images, including IKONOS, QuickBird, and WorldView-1. This mathematical model uses a pair of polynomial ratios to approximate the co-linearity equations. Due to its standardization and simplicity, this approach has been widely used in the remote-sensing community.

There are two possible ways to implement the RFM: the direct method (Tao and Hu 2002) and the bias-compensated method (Fraser and Hanley 2003). The direct RFM employs numerous ground control entities to determine the rational polynomial coefficients (RPCs). This approach requires many control entities to identify the parameters of high-order polynomial functions. The bias-compensated RFM first uses on-board data to calculate the RPCs and then uses a few ground control entities to refine the model. The bias-compensated method is more flexible than the direct method because most high-resolution satellites provide on-board data with high relative accuracy.

1.2. Related research

Previous studies adopting linear features for photogrammetric analysis primarily focus on the aerial frame camera. An example of this is the determination of image orientation parameters using linear features and vector maps (Karjalainen, Hyyppa, and Kuittinen 2006; Jaw and Perny 2008). Schenk (2004) combined collinearity and coplanarity models with linear features to achieve aerial triangulation. They simultaneously applied control lines and tie lines to perform bundle adjustment. Habib and Alruzouq (2004) adopted linear features as registration primitives for image registration. The concept of linear features is also applicable to camera calibration using self-calibration (Habib and Morgan 2005).

Due to improvements in spatial resolution, the control line concept is also applicable to high-resolution satellite images (Elaksher 2008). Shi and Shaker (2006) presented a line-based transformation model (LBTM) for IKONOS and QuickBird images. Their approach first reformats the two end points of control lines into unit vectors and then selects an affine transformation to describe the transformation between the unit vectors in two spaces. A single point is also needed to calculate the translation coefficients. Shaker (2007) extended this model to a 3D affine LBTM for terrain modelling. Samadzadegan, Saeedi, and Shenk (2006) presented a line-based generic model (LBGM) for IKONOS images. Their approach first reformats the two end points of control lines into polar parametric parameters and then selects the rational function model to describe the transformation between 2D image space and 3D object space.

1.3. The need for more investigation

Several investigators have used line-based direct RFM (Samadzadegan, Saeedi, and Shenk 2006) for high-resolution satellite imagery. However, relatively few studies discuss the bias-compensated RFM with control lines. The bias-compensated RFM with control lines uses the sensor-orientated RPCs from metadata to calculate the transformation between the object and uncorrected image spaces. This type of RFM then uses the control lines to compensate for errors between the object space and uncorrected image space. Sensor-orientated RPCs are generated from on-board data and provide high relative accuracy. Jacobsen (2008) compared direct RFM and bias-compensated RFM using control points for WorldView-1, QuickBird, IKONOS, OrbView-3, and Cartosat-1 images, indicating that the bias-compensated RFM reached sub-pixel accuracy with only a few control points. Therefore, the advantage of bias-compensated RFM is that it reduces the need for control entities.

1.4. The purposes

The primary objective of this study is to develop various line-based RFMs, i.e. a direct RFM and a bias-compensated RFM. This study also compares the performances of different line-based geometric correction models. The geometric correction models cover the control line, which utilized parametric and vector forms. For direct RFM, input data are control lines and output results are the transformation coefficients from 3D object space to 2D image space. The proposed scheme integrates line equations and RFM to solve the RPCs. For bias-compensated RFM, the input data are sensor-orientated RPCs and control lines and output results are the transformation coefficients from 3D object space to 2D image space. The bias-compensated RFM includes two major steps. First, the 3D lines in the object space are transformed to 2D lines in the image space using sensor-orientated RPCs. Then, the biases of RPCs are compensated by 2D transformation model using control lines. The experiments in this study analysed the effects of line number, orientation, and length using simulation and real data, including IKONOS and QuickBird images. Moreover, this study also compares the results of direct RFM and bias-compensated RFM using control lines.

2. The proposed scheme

The proposed line-based RFMs include direct RFM and bias-compensated RFM using control lines. This study develops and compares two line-based RFMs using different line

representations: (1) control line in parametric form and (2) control line in vector form. The following section provides the details of the proposed scheme.

2.1. Line representation

Control points are usually represented by the location of a point in a Cartesian coordinate system. Unlike the control point method, control lines represent a straight line in a Cartesian coordinate system or parametric system. The representations for a straight line include algebraic form, parametric form, and vector form. The representation typically used for a straight line is an algebraic form (Figure 1(*a*)). Equation (1) shows the algebraic form of a straight line. The line parameters include the slope and the *y*-intercept. Figure 1(*b*) shows an alternative representation in parametric form. Equation (2) shows the parametric form of a straight line. Figure 1(*c*) is a vector form with a starting point, direction, and scale. Equation (3) shows the corresponding vector form equation.

The line representations above adopt different parameters to present a straight line. These different parameters lead to the different mathematical models for RFM using control lines. This study does not apply an algebraic equation for line-based RFMs because it is not suitable to represent a vertical line. The other line representations are utilized in this study.

The accuracy of control entities is the most important issue when determining the influence of control entities in geometric correction. The number and distribution of control entities may also affect correction results. An additional requirement for control lines is the direction of lines. It is not necessary to have all the control lines in the same direction to obtain reliable results. In fact, the line-based RFM requires different line directions to avoid singular problem.

$$y = mx + c \tag{1}$$

$$\rho = x\cos\theta + y\sin\theta \tag{2}$$

$$\begin{bmatrix} x \\ y \end{bmatrix} = \begin{bmatrix} x_0 \\ y_0 \end{bmatrix} + s\begin{bmatrix} \mathrm{d}x \\ \mathrm{d}y \end{bmatrix}, \tag{3}$$

where x and y are the line coordinates, m is the slope parameter in algebraic form, c is the y-intercept in algebraic form, ρ is the perpendicular distance from origin to line in parametric form, θ is the angle of inclination of perpendicular with positive x-axis in parametric form, x_0 and y_0 are the starting points of a line in vector form, dx and dy are the directions of a line in vector form, and s is a scale factor.

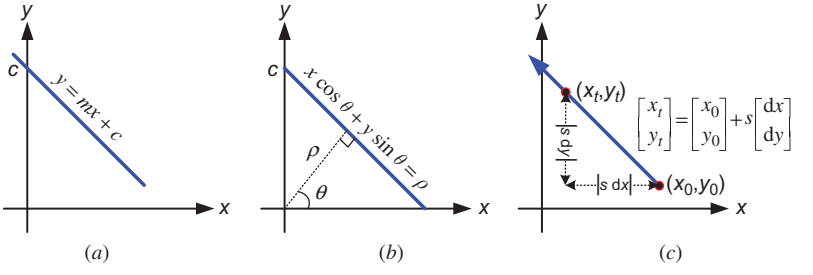

Figure 1. Line representations: (*a*) algebraic form, (*b*) parametric form, and (*c*) vector form.

2.2. Direct RFM using control lines

A RFM is a model describing the spatial relationship between the image space and object space. A RFM uses a pair of ratios of two polynomials to link the geometry between a 2D image point and the 3D corresponding object point, as shown in Equation (4). The RFM coefficients are called RPCs. This section presents the procedure of direct RFM using control lines. A control line contains a 2D line in the image space and a 3D line in the object space. Figure 2(*a*) illustrates a control line in the image and object spaces. Figure 2(*b*) shows that the two measured points on the line segments in the image and object spaces are not required to be conjugate points. Direct RFM utilizes the ground control lines (GCLs) to determine these coefficients, which are called GCL-derived RPCs:

$$x_r = \frac{P_1(X_g, Y_g, Z_g)}{P_2(X_g, Y_g, Z_g)} = \frac{\sum_{i=0}^{m1}\sum_{j=0}^{m2}\sum_{k=0}^{m3} a_{ijk} X_g^i Y_g^j Z_g^k}{\sum_{i=0}^{m1}\sum_{j=0}^{m2}\sum_{k=0}^{m3} b_{ijk} X_g^i Y_g^j Z_g^k},$$
$$y_r = \frac{P_3(X_g, Y_g, Z_g)}{P_4(X_g, Y_g, Z_g)} = \frac{\sum_{i=0}^{m1}\sum_{j=0}^{m2}\sum_{k=0}^{m3} c_{ijk} X_g^i Y_g^j Z_g^k}{\sum_{i=0}^{m1}\sum_{j=0}^{m2}\sum_{k=0}^{m3} d_{ijk} X_g^i Y_g^j Z_g^k}, \quad (4)$$

where x_r and y_r are the normalized image coordinates in RFM image space, X_g, Y_g, and Z_g are the normalized object coordinates in ground space, a_{ijk}, b_{ijk}, c_{ijk}, and d_{ijk} are the polynomial coefficients, and i, j, and k indicate the order of the polynomial functions, $0 \leq i, j, k \leq 3$ and $i + j + k \leq 3$.

2.2.1. Vector form

This section integrates the straight line equation and RFM for line-based RFM. Equation (4) shows the RFM. Equations (5) and (6) show the vector form line equations for the image and object spaces, respectively. Because the line equations can be represented in the image and object spaces, there are three possible methods to solve the GCL-derived RPCs using control lines. The first method is to establish line equations in both image and object

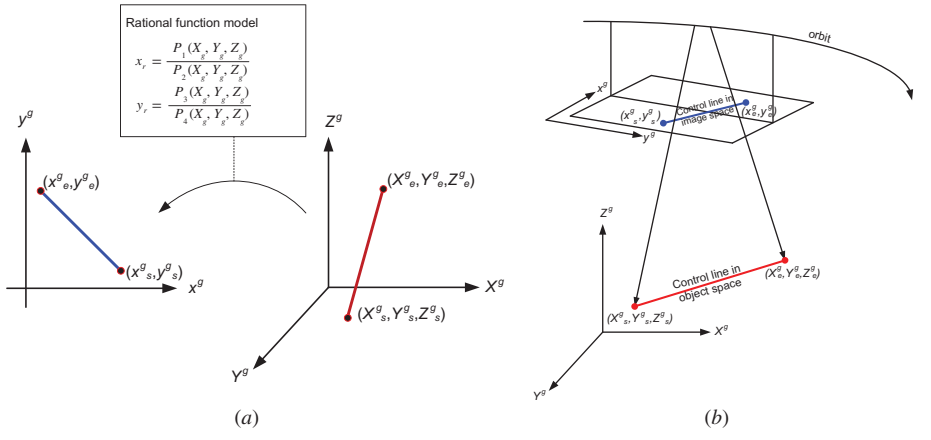

Figure 2. Illustration of direct RFM using a control line: (*a*) RFM between the control line in the vector image and object spaces (*b*) 3D view. The subscript s in $(x_s, y_s, X_s, Y_s, Z_s)$ indicates the starting point of a line while the subscript e in $(x_e, y_e, X_e, Y_e, Z_e)$ indicates the end point of a line.

spaces. This RFM can be rewritten with line equations, as shown in Equation (7). This approach causes a singular problem because many points located in both spaces may satisfy Equation (7). The second method uses the line equations in the object space and the corresponding image point in the image space. This RFM can be rewritten with vertices and line equations (Equation (8)). Equation (8) combines Equations (4) and (5). The idea behind this approach is to solve a scale factor t in the object space so that the vertices of the control line in both image and object spaces satisfy RFM. The third method represents a line in the image space and the corresponding object point in the object space. This RFM can be rewritten with vertices and line equations, as indicated in Equation (9). Equation (9) combines Equations (4) and (6) to obtain the observation equations for direct RFM using the control line. Equation (9) differs from Equation (8) in that the former determines the scale factor t in the image space, whereas the latter uses the scale factor s in the object space. The second and third models solve the GCL-derived RPCs using control lines. Comparing the second and third cases shows that the second case is more complicated. This is particularly true when using a parametric form to present a line. Hence, this study adopts the third model (i.e. Equation (9)).

For a rotating linear camera, the straight lines in the object space are not necessarily straight lines in the image space. Hence, the object line model in Equation (8) should be applied. For the spaceborne pushbroom linear camera used in this research, the geometric of the pushbroom linear camera is a perspective projection in the across-track direction and a parallel projection in the along-track direction. Hence, this study assumes that the straight line in the object space is also a straight line in the image space. In the across-track direction, the across-track field-of-view of a high-resolution satellite image is relatively small when compared with a frame camera, i.e. 0.93° for IKONOS and 2.12° for QuickBird. Therefore, the image distortion in a small area is linear behaviour. In the along-track direction, the length of the control line is relatively shorter than the image length. The sampling rate for a linear charge-coupled device (CCD) can be assumed to be constant in a short period. In other words, the acquisition of the pushbroom linear camera is uniform and stable in a short period. Thus, the effect of line distortion in the along-track direction is not significant.

The vector form coefficients (x_0, y_0, dx, dy) in Equation (9) can be calculated from the vertices of the control line in the image space. The unknowns of this model include the GCL-derived RPCs and the scale factor s from the line equation. The GCL-derived RPCs are used to determine the object-to-image transformation, whereas the additional scale factor s is used to determine the vertex of the control line in the image space. In most cases, the vertex of a control line is different in the image space and object space (e.g. Figure 2(b)). Thus, using a control line requires an additional scale factor s to find the corresponding image coordinates of the control line.

A control line with two vertices can lead to four observation equations. When the number of GCLs exceeds the number of observation equations, the proposed method uses least squares adjustment to solve the unknown parameters. The number of unknowns is the number of GCL-derived RPCs and scale factors. This equation minimizes the distance between the transformed vertices of a line from the object space and the corresponding line vertices in the image space. Figure 3 illustrates the minimization of this model.

$$\begin{aligned} X_g &= X_0 + t\,\mathrm{d}X \\ Y_g &= Y_0 + t\,\mathrm{d}Y \\ Z_g &= Z_0 + t\,\mathrm{d}Z, \end{aligned} \tag{5}$$

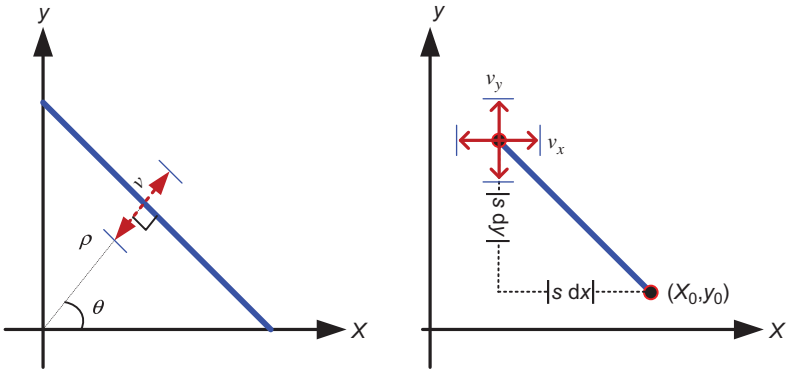

Figure 3. Comparison of vector and parametric forms for line-based RFM.

$$\begin{aligned} x_r &= x_0 + s\,\mathrm{d}x \\ y_r &= y_0 + s\,\mathrm{d}y, \end{aligned} \tag{6}$$

$$x_0 + s\,\mathrm{d}x = \frac{P_1(X_0 + t\,\mathrm{d}X, Y_0 + t\,\mathrm{d}Y, Z_0 + t\,\mathrm{d}Z)}{P_2(X_0 + t\,\mathrm{d}X, Y_0 + t\,\mathrm{d}Y, Z_0 + t\,\mathrm{d}Z)}$$

$$y_0 + s\,\mathrm{d}y = \frac{P_3(X_0 + t\,\mathrm{d}X, Y_0 + t\,\mathrm{d}Y, Z_0 + t\,\mathrm{d}Z)}{P_4(X_0 + t\,\mathrm{d}X, Y_0 + t\,\mathrm{d}Y, Z_0 + t\,\mathrm{d}Z)}, \tag{7}$$

$$x_r = \frac{P_1(X_0 + t\,\mathrm{d}X, Y_0 + t\,\mathrm{d}Y, Z_0 + t\,\mathrm{d}X)}{P_2(X_0 + t\,\mathrm{d}X, Y_0 + t\,\mathrm{d}Y, Z_0 + t\,\mathrm{d}X)}$$

$$y_r = \frac{P_3(X_0 + t\,\mathrm{d}X, Y_0 + t\,\mathrm{d}Y, Z_0 + t\,\mathrm{d}X)}{P_4(X_0 + t\,\mathrm{d}X, Y_0 + t\,\mathrm{d}Y, Z_0 + t\,\mathrm{d}X)}, \tag{8}$$

$$x_0 + s\,\mathrm{d}x = \frac{P_1(X_g, Y_g, Z_g)}{P_2(X_g, Y_g, Z_g)}$$

$$y_0 + s\,\mathrm{d}y = \frac{P_3(X_g, Y_g, Z_g)}{P_4(X_g, Y_g, Z_g)}, \tag{9}$$

where x_r and y_r are the image coordinates, X_g, Y_g, and Z_g are the object coordinates, x_0, y_0, X_0, Y_0, and Z_0 are the starting points of a line in vector form, dx, dy, dX, dY, and dZ are the directions of a line in vector form, and s and t are scale factors.

2.2.2. *Parametric form*

Equation (10) shows the 2D line equation in parametric form. The parameters ρ and θ in the line equation can be calculated from the vertices of the control line. The image coordinates (x_r and y_r) in Equation (10) can be substituted by RFM, as shown in Equation (4). Thus, Equation (11) presents the observation equation for direct RFM using a control line. The observation equation minimizes the error of the perpendicular distance. In other words, the equation states that the 2D line calculated from object coordinates should be collinear with 2D line in image coordinates. Figure 3 compares the minimization of parametric and vector

forms. The vertices of a control line in image and object spaces can be different, but the straight lines in the image and object spaces must be conjugate lines.

Each control line contains at least two vertices. Hence, a control line may establish two observation equations. The number of unknowns depends on the order of RFM. When the number of observation equations exceeds the number of unknowns, least square adjustment is conducted to compute the coefficients

$$\rho = x_r \cos\theta + y_r \sin\theta, \tag{10}$$

$$\rho = \frac{P_1(X_g, Y_g, Z_g)}{P_2(X_g, Y_g, Z_g)} \cos\theta + \frac{P_3(X_g, Y_g, Z_g)}{P_4(X_g, Y_g, Z_g)} \sin\theta, \tag{11}$$

where x_r and y_r are the image coordinates, X_g, Y_g, and Z_g are the object coordinates, ρ is the perpendicular distance from origin to line in parametric form, and θ is the angle of inclination of perpendicular with positive x-axis in parametric form.

2.3. Bias-compensated RFM using control lines

The bias-compensated RFM in this study utilized the sensor-orientated RPC provided by the satellite vendor. The sensor-orientated RPC was generated from the satellite's on-board orientation, including orbital parameters and attitude parameters. This study uses a sensor-orientated RPC to simplify complex physical sensor models, as most high-resolution satellites can provide precise on-board orientation. A sensor-orientated RPC describes the initial transformation between image and object spaces. However, its accuracy depends on the accuracy of on-board data. To improve the accuracy of image–object transformation model, this study adopts an additional mapping function to correct the biases in the image space.

The bias-compensated RFM includes two tasks: establishing the RFM and bias compensation in image space. Starting from the object space, the 3D object coordinates (X_g, Y_g, and Z_g) are mapped to the RFM coordinates (x_r and y_r) using sensor-orientated RPCs. The accuracy of the 2D image coordinates (x_g and y_g) can then be adjusted by the 2D affine transformation model in Equation (12). Figure 4 illustrates the concept of bias-compensated RFM using control lines

$$\begin{aligned} x_g &= A_{01} + A_{02}x_r + A_{03}y_r \\ y_g &= A_{11} + A_{12}x_r + A_{13}y_r, \end{aligned} \tag{12}$$

where x_r and y_r are the image coordinates determined by RFM, x_g and y_g are the image coordinates of control entities, and A_{01}–A_{13} are the affine coefficients.

2.3.1. Vector form

The first step of bias-compensated RFM is used to setup a line equation for a control line. Line equations can be presented in both image and object spaces. This study uses the image space control lines described in Section 2.2.1. Equation (13) shows the vector form of a control line in the image space. This equation can express any point on the control line in the image space. The image coordinates (x_g and y_g) in Equation (13) can be replaced by Equation (12). Hence, Equation (14) shows the observation equations for bias-compensated RFM using control lines

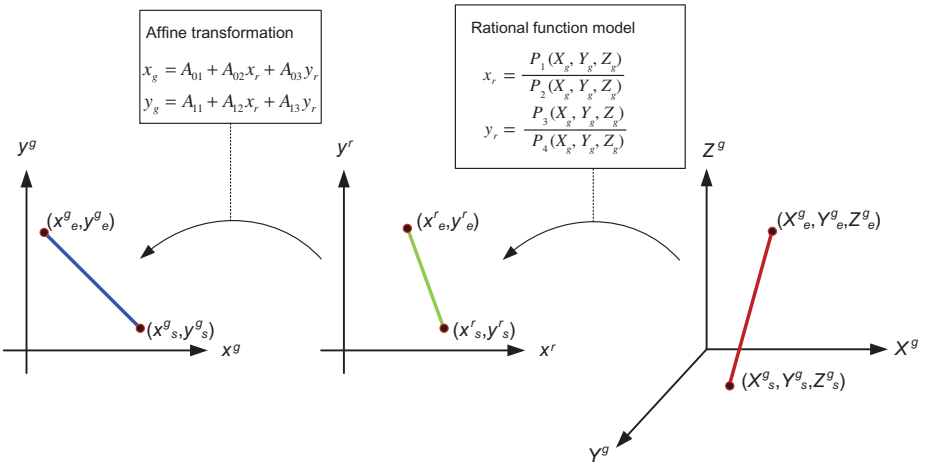

Figure 4. Illustration of bias-compensated RFM using control lines.

$$\begin{aligned} x_g &= x_0 + dx * s \\ y_g &= y_0 + dy * s, \end{aligned} \tag{13}$$

$$\begin{aligned} A_{01} + A_{02}x_r + A_{03}y_r &= x_0 + \mathrm{d}x * s \\ A_{11} + A_{12}x_r + A_{13}y_r &= y_0 + \mathrm{d}y * s. \end{aligned} \tag{14}$$

The line coefficients (x_0, y_0, dx, and dy) in Equation (14) are calculated from the vertices of control line in image space. The image coordinates in RFM space (x_r and y_r) are calculated from the object coordinates (X_g, Y_g, and Z_g) of the control line and sensor-orientated RPCs. The unknown parameters are the coefficients of affine transformation ($A_{01} \sim A_{13}$) and scale factor s. The coefficients of affine transformation compensate for the residuals of the RFM image space and control line image space. The scale factor s determines the image location for the control line vertices transformed from the object space. Hence, the measured and transformed control lines in the image space are collinear.

2.3.2. *Parametric form*

This study also uses the parametric form of the control line to perform the bias-compensated RFM. Equation (15) shows the parametric form in image space. The image coordinates (x_g and y_g) can be substituted into Equation (15) using the affine transformation in Equation (12). The observation equation can be written as Equation (16), in which the parameters of line (ρ,θ) are calculated from the control line vertices in the image space. The control line vertices (X_g, Y_g, and Z_g) in the object space were transformed to RFM coordinates (x_r and y_r) using the sensor-orientated RPCs. The control line in the RFM space (x_r and y_r) and image space (x_g and y_g) should be conjugate lines. So, each control line contains at least two vertices. Hence, a control line may establish two observation equations. There are six unknowns for this affine transformation. Least square adjustment is applied when the number of control lines exceeds three lines.

$$\rho = x_g \cos\theta + y_g \sin\theta, \tag{15}$$

$$\rho = (A_{01} + A_{02}x_r + A_{03}y_r)\cos\theta + (A_{11} + A_{12}x_r + A_{13}y_r)\sin\theta. \tag{16}$$

Table 1. Comparison of direct and bias-compensated RFM using control lines.

	Direct RFM		Bias-compensated RFM	
Items	Vector form	Parametric form	Vector form	Parametric form
Pre-knowledge	No	No	Sensor-orientated RPCs	Sensor-orientated RPCs
Unknown parameters	1. GCL-derived RPCs 2. Scale factor	1. GCL-derived RPCs	1. Coefficients of affine 2. Scale factor	1. Coefficients of affine
Minimum number of control lines	7 (order = 1) 19 (order = 2) 39 (order = 3)	7 (order = 1) 19 (order = 2) 39 (order = 3)	3	3
Non-linear equation	Yes	Yes	No	No
Advantage	Pre-knowledge parameters are not required.		The need of the number of control line is less than direct RFM.	
Disadvantage	The required control line is more than bias-compensated RFM.		Sensor-orientated RPCs are required.	

2.4. Comparison

Table 1 compares the direct RFM and bias-compensated RFM. Both methods are based on RFM. The major difference between these two models is that the bias-compensated RFM needs sensor-orientated RPCs, whereas direct RFM does not require these parameters. In direct RFM, the control line determines the RPCs that describe the relationship between object and image space. Unlike direct RFM, the control line in bias-compensated RFM is to correct the bias of sensor-orientated RPCs. Thus, bias-compensated RFM requires fewer control lines than direct RFM. Although line equations in vector form require additional scale parameters to determine the image location of transformed vertices, the minimum number of control lines is the same as the parametric form. Both line representations provide similar results.

3. Experimental results

The experiments in this study used simulation and real data to analyse the performance of line-based RFMs. This study simulates GCLs and independent check points (ICPs) in different combinations to compare both models thoroughly. After analysing simulation data, IKONOS and QuickBird images were selected to provide the numerical experimental results of the proposed methods.

3.1. Simulation data

The line-based RFMs include direct RFM and bias-compensated RFM using control lines. The simulation in this study was based on a sensor model of a pushbroom satellite image. This study uses a sensor model to generate a large number of GCLs and ICPs. The simulation added 0.5 pixels and 0.5 m random error to the vertices of GCLs in both image and object spaces. One thousand ICPs were simulated to check the accuracy of different GCL combinations. The ICP coordinates were assumed to have no random errors because

Table 2. Comparison of direct and bias-compensated RFM using control line.

No	Evaluation item	Parameters			
		Random error	Number of GCLs	Length (m)	Angle between GCLs (°)
1	Effect of the total number of GCLs	0.5 m/0.5 pixel	5×5×5∼10×10×10*	30	90
2	Effect of the angle between GCLs	0.5 m/0.5 pixel	5×5×5	30	10∼90**
3	Effect of the length of GCLs	0.5 m/0.5 pixel	5×5×5	10∼100***	90

Notes: *Numbers of GCLs (m): 125, 216, 343, 512, 729, and 1000.
**Angles of GCLs (°): 10, 20, 30, 40, 50, 60, 70, 80, and 90.
***Lengths of GCLs (m): 10, 20, 30, 40, 50, 60, 70, 80, 90, and 100.

the residuals of ICPs are defined as the accuracy of proposed methods. The 2D root mean squares error ($RMSE_{2D}$) in Equation (17) was calculated for each model as an accuracy index (Aguilar et al. 2008). The number of GCLs, the angle between GCLs, and the length of GCLs are the three most important factors in line-based RFM. Table 2 shows the three combinations of simulation data.

$$RMSE_{2D} = \sqrt{RMSE_x^2 + RMSE_y^2}, \tag{17}$$

where $RMSE_x$ and $RMSE_y$ are the RMSE values in the x and y directions, respectively.

To evaluate the influence of the GCLs numbers on line-based RFM accuracy, the GCLs were distributed on 3D object grids. The numbers of control lines varied from 5×5×5 to 10×10×10 lines, whereas the GCL length remained fixed at 30 m in the object space. The azimuth angles for GCLs were 0 or 90°, which means the angle between GCLs was fixed as 90° in a well condition. Figure 5 shows the accuracy of ICPs for different models when different numbers of GCLs were applied. This figure shows that the accuracy of ICPs improved as the number of GCLs increased. The bias-compensated RFM was more stable than the direct RFM when GCLs were applied. The second-order line-based RFM was better than the first-order line-based RFM. The vector and parametric forms behaved similarly.

A comparison of control point and control lines shows that the control point only considers the number and distribution of points, but the control line considers the number, distribution, and orientation of lines. The angles between GCLs were distributed from 10 to 90° to evaluate the influence of the GCLs orientation. Figure 6 shows the accuracy due to the orientation angle given 125 GCLs. The control capability of GCLs improved when the line orientation neared 90°. This suggests that when the angle between GCLs exceeds 45°, the accuracy is less than 1 pixel for different angles. The bias-compensated RFM was more stable than the direct RFM because the bias-compensated RFM utilized sensor-orientated RPCs in the initial transform.

This study also evaluates the accuracy of ICPs when different lengths of GCLs are applied. The simulated lines ranged from 10 to 100 m long. The angle between GCLs remained fixed at 90°, and the number of lines was 125. Assuming that long lines are more reliable than short lines, the longest lines should have the lowest measurement errors. Hence, this study simulated GCLs with different measurement errors from 0.1 to 1.0 pixels.

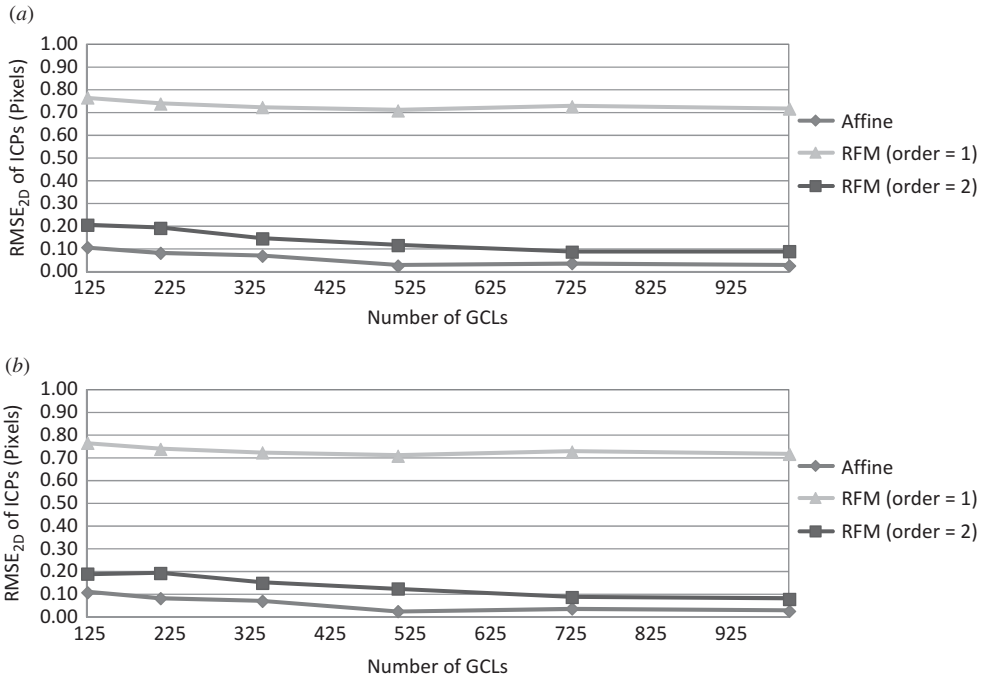

Figure 5. Evaluation of the number of GCLs: (*a*) parametric form and (*b*) vector form.

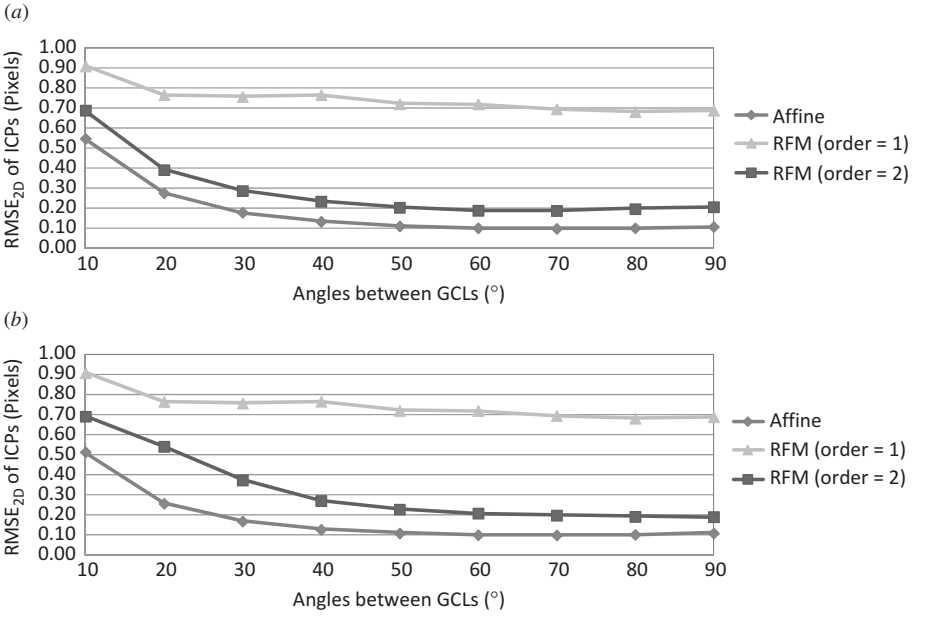

Figure 6. Evaluation of the angle between GCLs: (*a*) parametric form and (*b*) vector form.

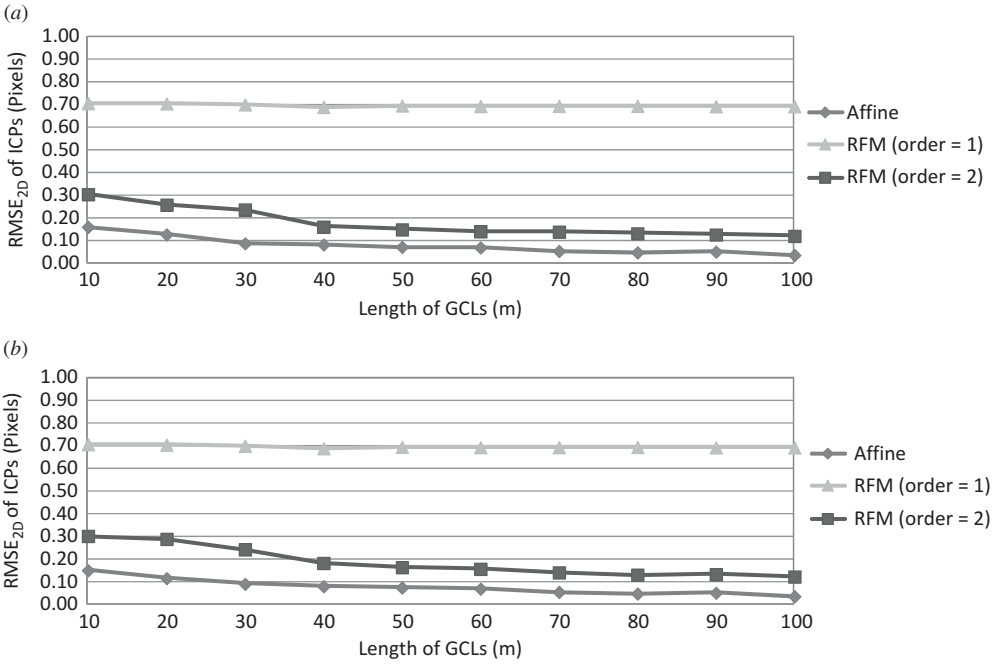

Figure 7. Evaluation of the length of GCLs: (*a*) parametric form and (*b*) vector form.

Figure 7 shows the simulation results, indicating that the effect of length is relatively more stable than the effect of angles. A longer line with smaller measurement errors yields more accurate results. The parametric and vector forms behaved similarly.

3.2. Real images

The test images were IKONOS and QuickBird satellite images. The GCLs were measured from 3D building models, as shown in Figure 8(*a*). This study used the ICPs to evaluate the accuracy of different models. The ICPs were measured from the control point database with a position accuracy of 50 cm. Table 3 lists the number of GCLs and ICPs and related information. Figures 8(*b*) and (*c*) show the distributions of these GCLs and ICPs for IKONOS and QuickBird, respectively. The lines in these figures represent the GCLs, while the circles represent the ICPs. Figure 9 shows an example of control lines. The lines in these figures represent the image location of control lines. The control lines were located along a ridge or building boundary.

The experiment using real data analysed from two different aspects. The first aspect compared the accuracies of direct RFM and bias-compensated RFM using GCLs, whereas the second aspect compared different line representations in vector and parametric forms. This study uses the same GCLs and ICPs to compare the accuracies of direct RFM and bias-compensated RFM. The line-based direct RFM includes first-order and second-order RFMs. The line-based bias-compensated RFM utilizes the affine transformation and sensor-orientated RPCs from metadata. Hence, three mathematical models were included in the comparison. Different numbers of GCLs were used to calculate the coefficients, and the same number of ICPs was used to verify accuracy.

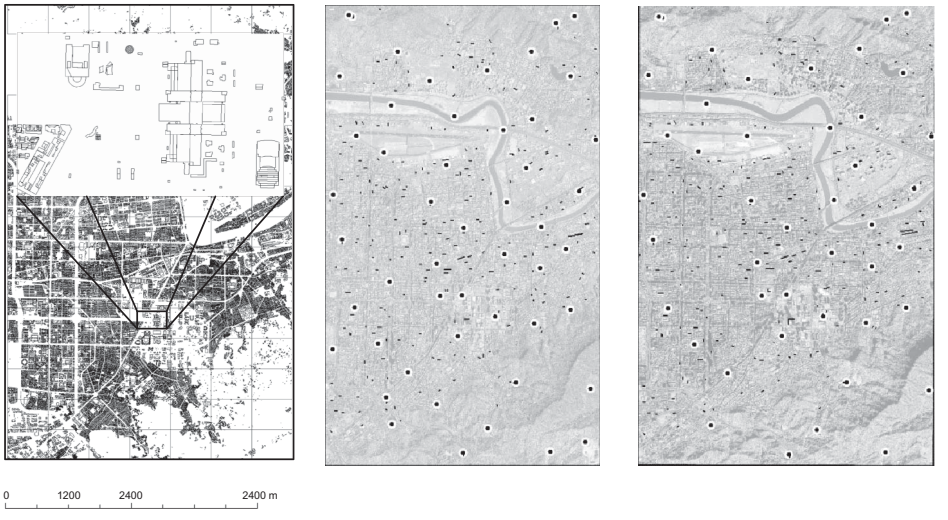

(*a*) (*b*) (*c*)

Figure 8. The test data: (*a*) 3D building models, (*b*) configurations of the GCLs and ICPs in the IKONOS image, and (*c*) configurations of the GCLs and ICPs in the QuickBird image.

Table 3. Related information for the test images.

	Case I	Case II
Sensor	IKONOS	QuickBird
Location	Taipei, Taiwan	Taipei, Taiwan
Level	Geo	Standard
Acquisition date	21 February 2002	15 December 2002
GSD (m)	1.00	0.67
Spectral information	Pan	Pan
Elevation angle (°)	63.34	68.6
Azimuth angle (°)	224.68	268.9
Image size (km × km)	5.6 × 9.6	5.6 × 9.6
Number of GCLs	242	251
Number of ICPs	40	40

Figure 10 shows the accuracy analysis for an IKONOS image. The number of GCLs ranged from 24 to 251 lines, whereas the number of ICPs remains fixed at 40 points. Figure 10(*a*) compares the accuracies of these three models in vector form, clearly showing that bias-compensated RFM achieves higher accuracy and provides more stable results. The $RMSE_{2D}$ of ICPs is better than 1.05 pixel for bias-compensated RFM. The accuracy of second-order RFM improved from 1.10 to 1.04 pixels as the number of GCLs increased from 24 to 251. The accuracy of second-order RFM is better than first-order RFM. This behaviour is similar to that observed in simulation one. This is likely because the satellite image requires more RPCs to describe the relationship between the object and image spaces. Figure 10(*b*) compares the accuracies of different line-based RFMs in the parametric form. The GCLs and ICPs for vector and parametric forms are the same. Hence, the results of these two line representations are similar. In other words, when the measurement error of GCLs is similar, the results of line-based RFMs using vector and parametric forms have similar accuracies.

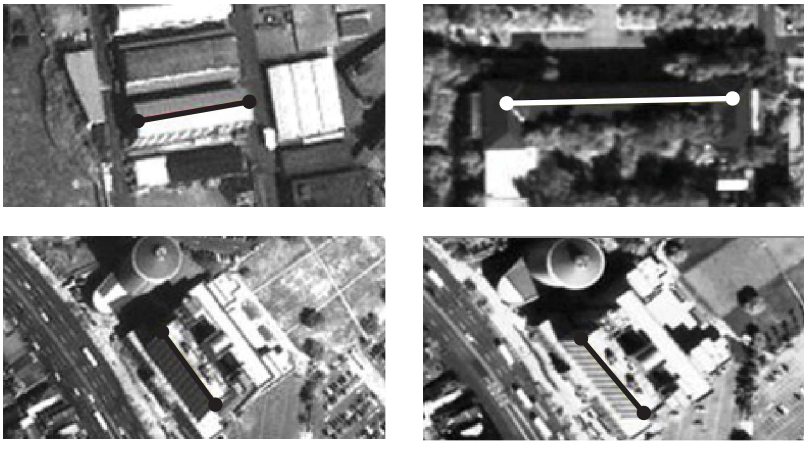

(*a*) (*b*)

Figure 9. Examples of control lines: (*a*) GCLs in the IKONOS image and (*b*) GCLs in the QuickBird image.

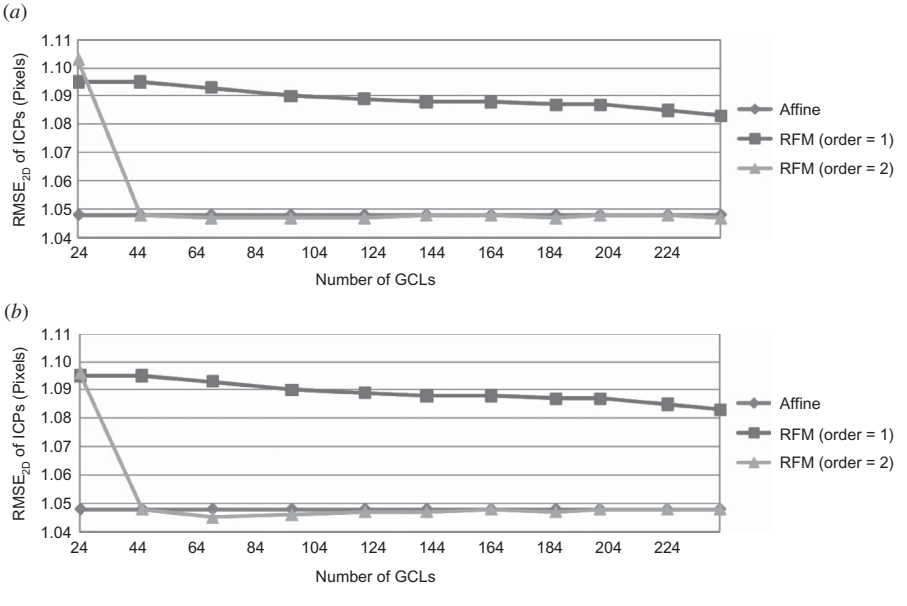

Figure 10. Accuracy analysis for the IKONOS satellite image using control lines: (*a*) vector form and (*b*) parametric form.

Figure 11 summarizes the accuracies of the QuickBird image. This study uses different numbers of GCLs to perform line-based RFM. The numbers of GCLs are ranged from 24 to 244 lines, whereas the number of ICPs remained at 40. Figure 11(*a*) shows the results of three different models. The RMSEs of ICPs for the first-order RFM are from 1.80 to 1.54 pixels. The second-order RFM is better than the first-order RFM. The second-order accuracies range from 1.27 to 1.17 pixels. The second-order accuracies tend to stabilize when the number of GCLs exceeds 64. Bias-compensated RFM is more stable than second-order RFM when the number of GCLs is less than 64 because the unknowns

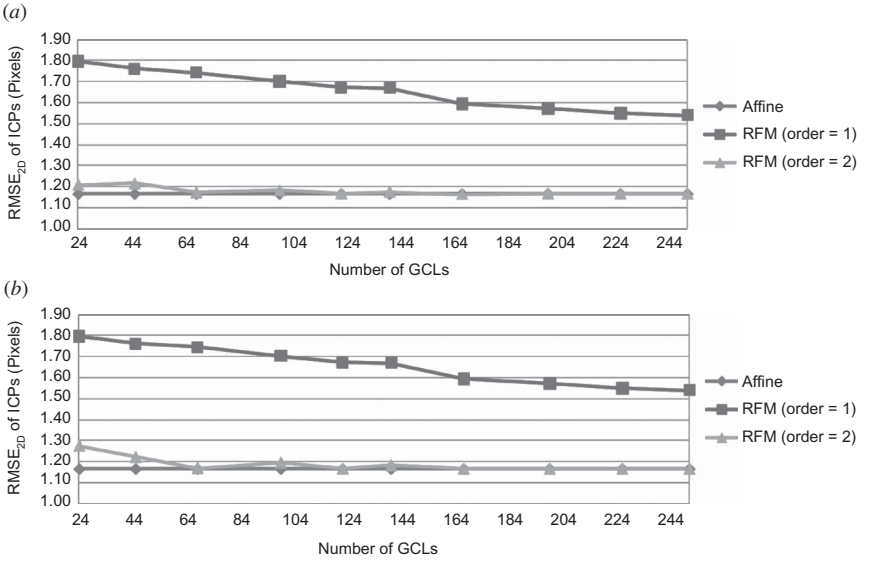

Figure 11. Accuracy analysis for the QuickBird satellite image using control lines: (*a*) vector form and (*b*) parametric form.

Table 4. Accuracy analysis of IKONOS and QuickBird images.

Unit: Pixel		Direct RFM (Order = 1)			Direct RFM (Order = 2)			Bias-compensated RFM (Affine)		
Sensor	Type	RMSE *x*	RMSE *y*	RMSE 2D	RMSE *x*	RMSE *y*	RMSE 2D	RMSE *x*	RMSE *y*	RMSE 2D
IKONOS	Vector	0.753	0.779	1.083	0.719	0.762	1.048	0.719	0.762	1.048
IKONOS	Parametric	0.753	0.779	1.083	0.719	0.762	1.048	0.719	0.762	1.048
QuickBird	Vector	1.295	0.833	1.540	0.882	0.764	1.166	0.881	0.764	1.167
QuickBird	Parametric	1.296	0.832	1.540	0.882	0.763	1.166	0.881	0.764	1.167

and bias-compensated RFM (i.e. 6) is less than the second-order RFM (i.e. 38). Since bias-compensated RFM utilizes the sensor-orientated RPCs from metadata, it achieves higher accuracy. Figure 11(*b*) shows the results of line-based RFM using the parametric form. The behaviors of the parametric form are similar to the vector form. In other words, whether the GCLs are presented in vector form or parametric form, they have similar accuracies.

Table 4 summarizes the results of these two cases when all GCLs are applied. The results of this experiment show that subpixel accuracy can be achieved by applying second-order RFM and bias-compensated RFM. This agrees with previous research, which shows that the accuracy of IKONOS and QuickBird may reach 1 pixel (Aguilar et al. 2008).

Since the results obtained from second-order RFM and bias-compensated RFM were similar, this study selects bias-compensated RFM to perform the registration of 3D building models and high-resolution satellite images. Figure 12 superimposes satellite images over 3D building models using the calculated coefficients. Figures 12(*a*) and (*b*) show two enlargements of IKONOS and QuickBird images, respectively, for ease of comparison. These figures show that the building models and satellite images fit quite well. The building

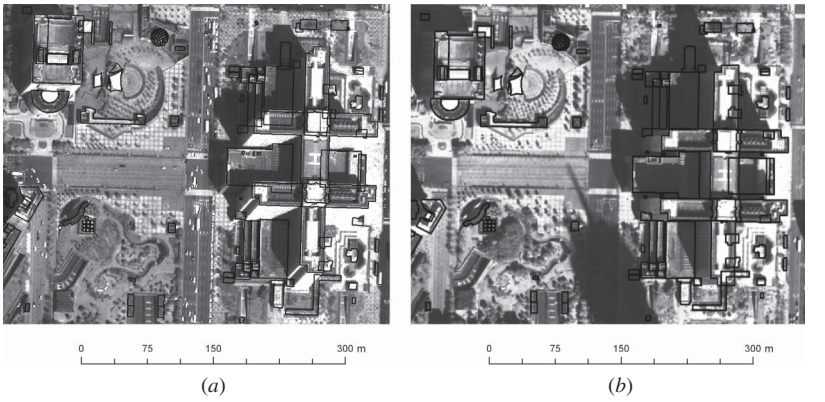

(*a*) (*b*)

Figure 12. Registration of building models and images: (*a*) IKONOS and (*b*) QuickBird.

boundaries are located at the correct locations, indicating that the proposed methods are able to provide highly accurate image-to-vector registration.

4. Conclusions

This study proposes mathematical models of a line-based rational function model. The proposed methods include direct RFM and bias-compensated RFM using control lines. Direct RFM obtains the RPCs directly from control lines, while bias-compensated RFM used sensor-orientated RPCs and control lines to obtain compensated coefficients. Control lines can be represented in vector and parametric forms. The vector form of control line represents the line in a Cartesian coordinate system using a starting point and scales. However, the parametric form of control line represents the line in parametric space using distance and angle.

The proposed methods can be utilized to register vector data and high-resolution images. The experiments in this study use simulation and real data to show that the angle between control lines and number of control lines are the two most important factors. Increasing the angle and number will improve accuracy. The experiments in this study used IKONOS and QuickBird images to evaluate the proposed methods. Experimental results indicate that the vector and parametric forms behave similarly. Both line representations can be applied to the line-based RFM, but the parametric form has fewer unknown parameters and is mathematically easier to solve. Bias-compensated RFM is more stable than direct RFM because the sensor-orientated RPCs for bias-compensated RFM have good relative accuracy. In other words, bias-compensated RFM does not require as many control lines when sensor-orientated RPCs are available. For the absolute accuracy from ICPs, the second-order RFM and bias-compensated RFM may reach subpixel accuracy when sufficient control lines are applied.

Future research on this topic should focus on automatic control line extraction to improve the automation of image-to-model registration. Line-based RFM for non-straight lines is another area for future research.

Acknowledgements

This study was supported in part by the National Science Council of Taiwan under Project NSC 99-2221-E-009-131. The author would like to thank the Centre for Space and Remote Sensing Research at National Central University in Taiwan for providing the test data sets.

References

Aguilar, M. A., F. Aguilar, F. J. Aguera, and F. Carvajal. 2008. "Geometric Accuracy Assessment of the Orthorectification Process from Very High Resolution Satellite Imagery for Common Agricultural Policy Purposes." *International Journal of Remote Sensing* 29: 7181–97.

Akav, A., G. H. Zalmanson, and Y. Doytsher. 2004. "Linear Feature Based Aerial Triangulation." *International Archives of Photogrammetry, Remote Sensing and Spatial Information Sciences* 35: 7–12.

Al-Ruzouq, R. I. 2010. "Data Fusion of Multi-Source Imagery Based on Linear Features Registration." *International Journal of Remote Sensing* 31: 5011–21.

Elaksher, A. F. 2008. "Developing and Implementing Line-Based Transformation Models to Register Satellite Images." *International Archives of Photogrammetry, Remote Sensing and Spatial Information Sciences* 37: 229–34.

Fraser, C. S., and H. B. Hanley. 2003. "Bias Compensation in Rational Functions for IKONOS Satellite Imagery." *Photogrammetric Engineering and Remote Sensing* 69: 53–7.

Grussenmeyer, P., and O. Al Khalil. 2002. "Solutions for Exterior Orientation in Photogrammetry: A Review." *Photogrammetric Record* 17: 615–34.

Habib, A. F., and R. I. Al-Ruzouq. 2004. "Line-Based Modified Iterated Hough Transform for Automatic Registration of Multi-Source Imagery." *Photogrammetric Record* 19: 5–21.

Habib, A., M. Ghanma, M. Morgan, and R. Al-Ruzouq. 2005. "Photogrammetric and Lidar Data Registration Using Linear Features." *Photogrammetric Engineering and Remote Sensing* 71: 699–707.

Habib, A. F., M. Morgan, and Y. R. Lee. 2002. "Bundle Adjustment with Self-Calibration Using Straight Lines." *Photogrammetric Record* 17: 635–50.

Jacobsen, K. 2008. "Satellite Image Orientation." *International Archives of Photogrammetry, Remote Sensing and Spatial Information Sciences* 37: 703–9.

Jaw, J. J. 2000. "Control Surface in Aerial Triangulation." *International Archives of Photogrammetry, Remote Sensing and Spatial Information Sciences* 33: 444–51.

Jaw, J. J., and N. H. Perny. 2008. "Line Feature Correspondence between Object Space and Image Space." *Photogrammetric Engineering and Remote Sensing* 74: 1521–28.

Jung, F., and D. Boldo. 2004. "Bundle Adjustment and Incidence of Linear Features on the Accuracy of External Calibration Parameters." *International Archives of Photogrammetry, Remote Sensing and Spatial Information Sciences* 35: 19–24.

Karjalainen, M., J. Hyyppa, and R. Kuittinen. 2006. "Determination of Exterior Orientation Using Linear Features from Vector Maps." *Photogrammetric Record* 21: 329–41.

Poli, D., L. Zhang, and A. Gruen. 2004. "Orientation of Satellite and Airborne Imagery from Multi-Line Pushbroom Sensors with a Rigorous Sensor Model." *International Archives of Photogrammetry, Remote Sensing and Spatial Information Sciences* 35: 130–5.

Samadzadegan, F., S. Saeedi, and T. Shenk. 2006. "A Feature Based Generic Model for Georeferencing of High Resolution Satellite Imagery." Paper presented at the 2nd WSEAS International Conference on Remote Sensing, Canary Islands, Spain, December 16–18.

Schenk, T. 2004. "From Point-Based to Feature-Based Aerial Triangulation." *ISPRS Journal of Photogrammetry and Remote Sensing* 58: 315–29.

Shaker, A. 2007. "Feature-Based Transformation Models for Satellite Image Orientation and Terrain Modeling." In *Proceedings of the ASPRS 2007 Annual Conference*, Tampa, FL, May 7–11, CD-Rom.

Shi, W. Z., and A. Shaker. 2006. "The Line-Based Transformation Model LBTM for Image-to-Image." *International Journal of Remote Sensing* 27: 3001–12.

Tao, C. V., and Y. Hu. 2002. "3D Reconstruction Methods Based on the Rational Function Model." *Photogrammetric Engineering and Remote Sensing* 68: 705–14.

Zitova, B., and J. Flusser. 2003. "Image Registration Methods: A Survey." *Image and Vision Computing* 21: 977–1000.